Available online at www.sciencedirect.com
SCIENCE DIRECT
International Journal of Multiphase Flow 32 (2006) 323–343
International Journal of Multiphase Flow
www.elsevier.com/locate/ijmulflow

Experimental study on oil–water flow in horizontal and slightly inclined pipes

O.M.H. Rodriguez *, R.V.A. Oliemans

J.M. Burger Centre for Fluid Mechanics, Kramers Laboratorium, Delft University of Technology, Prins Bernhardlaan 6, 2628 BW Delft, The Netherlands

Received 24 July 2005; received in revised form 6 November 2005

Abstract

Oil–water two-phase flow experiments were conducted in a 15 m long, 8.28 cm diameter, inclinable steel pipe using mineral oil (density of 830 kg/m^3 and viscosity of 7.5 mPa s) and brine (density of 1060 kg/m^3 and viscosity of 0.8 mPa s). Steady-state data on flow patterns, two-phase pressure gradient and holdup were obtained over the entire range of flow rates for pipe inclinations of $-5°$, $-2°$, $-1.5°$, $0°$, $1°$, $2°$ and $5°$. The characterization of flow patterns and identification of their boundaries was achieved via observation of recorded movies and by analysis of the relative deviation from the homogeneous behavior. A stratified wavy flow pattern with no mixing at the interface was identified in downward and upward flow. Two gamma-ray densitometers allowed for accurate measurement of the absolute in situ volumetric fraction (holdup) of each phase for all flow patterns. Extensive results of holdup and two-phase pressure gradient as a function of the superficial velocities, flow pattern and inclinations are reported. The new experimental data are compared with results of a flow pattern dependent prediction model, which uses the area-averaged steady-state two-fluid model for stratified flow and the homogeneous model for dispersed flow. Prediction accuracies for oil/water holdups and pressure gradients are presented as function of pipe inclination for all flow patterns observed. There is scope for improvement for in particular dual-continuous flow patterns.

Keywords: Liquid–liquid flow; Oil–water flow; Large diameter; Slightly-inclined pipe; Flow patterns; Holdup; Pressure gradient; Mechanistic model

1. Introduction

For most oil reservoirs we know that oil is seldom produced alone, but together with water and gas. In multiphase oil/gas production logging analysis, which is one of the most important aspects of managing oil/gas production of a field, one would like to derive for each well from limited down-hole information on

* Corresponding author. Present address: Depto. Engenharia Mecânica, Escola de Engenharia de São Carlos, Universidade de São Paulo (USP) Av. Trabalhador San-carlense, 400, 13566-970, São Carlos-SP, Brazil. Tel.: +55 16 3373 8026; fax: +55 16 3373 9402.
E-mail address: oscarmhr@sc.usp.br (O.M.H. Rodriguez).

0301-9322/$ - see front matter © 2005 Elsevier Ltd. All rights reserved.
doi:10.1016/j.ijmultiphaseflow.2005.11.001

phase holdup and pressure loss the oil, gas and water production rates one can expect. In modern reservoir management production occurs quite often from near-horizontal wells. Three-phase oil/water/gas flows in such near-horizontal wells is rather complex. The fluids can adopt different spatial configurations, known as flow patterns, each with its own slip relation, i.e., its own way to compute phase holdups and three-phase pressure loss. For the simpler case of purely horizontal oil/water pipe flow it has been shown recently (Rodriguez et al., 2004) that it is possible to derive from holdup and pressure gradient measurements oil and water superficial velocities via an inverse mode prediction technique.

In order to reconstruct the oil and water superficial velocities or production rates, from holdup and pressure gradient information, a flow-pattern-dependent model has been chosen as modeling approach. Although multiple solutions are expected in this kind of approach, since it is not a well-posed problem, for practical applications the range of solutions may be sufficiently small to obtain a practical estimate of the flow rates. The first step was the direct modeling, i.e., a suitable flow-pattern-dependent model for holdup and pressure gradient had to be identified. For that purpose we have started by using the simplest models that are available. Of course in a later phase improvements are required, since the better the direct modeling, the better the inverse mode predictions.

There are only a modest number of publications that address flow pattern transitions in liquid–liquid systems (Brauner and Maron, 1992a,b, 1999; Trallero, 1995; Trallero et al., 1997; Brauner, 2001; Rodriguez and Bannwart, 2004). The liquid–liquid flow-pattern prediction model proposed by Trallero (1995) was considered as a starting point for this work.

Several methods for calculating the pressure drop and the in situ volumetric fractions of the phases in pipelines have been published, which require a correct prediction of the flow patterns (Nädler and Mewes, 1997; Angeli and Hewitt, 1998). As another example, the modeling of corrosion-inhibitor transport in multiphase pipelines also involves determining the structure of the two-phase flow (Fairuzov, 2001; Fairuzov et al., 2000). In recent papers, Sotgia and Tartarini (2001) and Lovick and Angeli (2004) presented studies about the state of the art in horizontal oil–water flow (including viscous oils) and showed that there are still many discrepancies in two-phase pressure drop prediction. Even for the relatively simpler case when the oil viscosity is only a few times higher than water, there is no definitive model or correlation for predicting the two-phase pressure drop (Angeli and Hewitt, 1998; Valle and Utvik, 1997; Lovick and Angeli, 2001). In this study we use the standard area-averaged steady-state two-fluid model for stratified flow and the homogeneous model for dispersed flow for holdup and two-phase pressure gradient calculations. These have been chosen for their simplicity and reasonable accuracies when applied to horizontal oil–water flows of interest to this work (Rodriguez et al., 2004).

Oil–water data from literature to validate the inverse technique are rather scanty. Table 1 summarizes the data sets we have used for that purpose (Trallero, 1995; Alkaya et al., 2000; Fairuzov et al., 2000; Elseth, 2001; Oddie et al., 2003; a more extensive survey over less recent works on oil–water flow can be found in Lovick and Angeli, 2004). From the table it is clear that only Trallero (1995) and Elseth (2001) offer holdup and pressure gradient data for various flow patterns, but for horizontal flow only. Alkaya et al. (2000) investigated experimentally the effect of inclination angle on flow pattern transition boundaries in a slightly inclined

Table 1
Recent experimental works on larger diameter oil–water flow

	Alkaya et al. (2000)	Elseth (2001)	Oddie et al. (2003)	Trallero (1995)	Fairuzov et al. (2000)
Oil density, ρ_o (kg/m^3)	850	790	810	884	851
Oil viscosity, μ_o (mPa s)	17.9	1.64	1.5	28.8	5
Pipe diameter, D (cm)	5	5.63	15.2	5.01	36.35
Roughness (m)	10^{-5} [a]	10^{-5} [a]	10^{-5} [a]	10^{-5} [a]	7×10^{-5} [c]
Surface tension, σ (N/m)	0.036	0.043	0.017 [b]	0.036	0.036
Inclination angle, θ (°)	−5, −1, 0, 1 and 5	0	−2, 2, 0, 10 and 20	0	0
ΔP (Pa/m) and holdup (ε_w) data	No	Yes	No	Yes	No

[a] Acrylic (Plexiglas).
[b] Properties of the fluids similar to those in Angeli and Hewitt (1998).
[c] Steel.

5 cm i.d. pipe (−5 to +5), but do not provide holdups and pressure losses. Oddie et al. (2003) studied two and three-phase flows in a large inclined pipe (15 cm i.d.). Considering the liquid–liquid flow only, flow pattern characterization and holdup data (no pressure loss) for just two different upward inclinations are reported (+45 and +90, from the horizontal). Fairuzov et al. (2000) carried out full-scale experiments and reported flow pattern transitions only in a horizontal pipeline (36.35 cm i.d.) conveying oil–water mixtures. The flow pattern, holdup and pressure drop models proposed in this work have been validated for all the typical cases shown in Table 1 (Rodriguez et al., 2004).

We could not find quantitative data on the effects of the inclination angle on the pressure drop and holdup for the oil–water flow patterns and properties considered of interest for the production of oil and water from near-horizontal wells (with oil–water density ratio and viscosity ratio up to 0.75 and 30, respectively, mixture velocities up to 2 m/s in 5 up to 10 cm i.d. pipes and inclination angles from −5 to +5 from the horizontal). Therefore, the main goal of this work has been to collect a comprehensive set of oil–water flow data in a well-instrumented large-scale experimental apparatus for validation and extension of flow-pattern-dependent holdup and pressure gradient models. The data had to be of sufficient quality and quantity for practical use and for support of the development of new models. The experimental setup must allow for the observation of all flow patterns so far reported in the literature and be suitable to study the characteristics of each one at different deviations from horizontal.

The experimental results reported in the present study fill some of the gaps identified above. A set of liquid–liquid flow data was acquired in a horizontal and slightly inclined large steel pipe using mineral oil and brine. The following deviations from horizontal were studied: −5°, −2°, −1.5°, +1°, +2° and +5°. For horizontal flow and for each of the six inclinations we have collected data on two-phase pressure gradient, in situ volumetric fraction of the liquid phases (holdup) and on-line digital images of the flow. The holdup and pressure gradient data are presented as a function of the flow patterns, superficial velocities and inclinations, covering the entire range of flow rates.

2. Experimental setup

2.1. Inclinable flow loop

The experiments reported in this paper were performed at the Multiphase Test Facility of Shell Exploration and Production B.V., Rijswijk. Oil–water flow was investigated in a 3-in. 15-m long stainless steel pipe (roughness 4.5×10^{-5}). Stainless steel pipes (AISI-316L, schedule 10 S mm, i.d. = 82.5 mm) are used for the transport of the phases and mixtures. At the 15 m-long test section there is a 1.15 m-long transparent Perspex (PMMA—polymethyl methacrylate) pipe section for visualizations. The large inclinable flow loop basically consists of the pipe-work represented in Fig. 1. A mixing section is responsible for the generation of the multiphase flow (Fig. 1a). In between the mixing section and the test section a length of 250 D is left for the two-phase flow development. As a matter of fact, only 35 D of straight line is left just before the test section, since the 250 D pipe length includes one turn back and two smooth 90° bends. The test section (Fig. 1b) is fixed to a table that can be pneumatically deviated from 0° (horizontal) to 90° (upright). The direction of the flow can be inverted; therefore the entire range of uphill and downhill flows can be investigated. Finally, the oil–water flow is conveyed to a separator.

2.2. Fluids, pumps and separator

Both water (brine, average density of 1060 kg/m^3 and viscosity of 0.8 mPa s) and oil (Shell Vitrea 10, average density of 830 kg/m^3 and viscosity of 7.5 mPa s) were kept in the same large separator (oil–water interfacial tension of 0.0204 N/m, brine–air and oil–air superficial tensions of 0.0507 N/m and 0.0303 N/m, respectively). Because of the difference in density oil lies in the upper part of the separator, while water remains in the lower part. Each phase was conveyed through its own series of pipes, pumps (2× Rheinhutte, RN 50/315B centrifugal pump), flow and temperature meters from the separator to the mixing section. The mixing section was a 2-m pipe section at which the oil and water lines were connected through independent valves. At the outlet of the test section pipes carried the mixture back to the separator. In case of dealing with three-phase

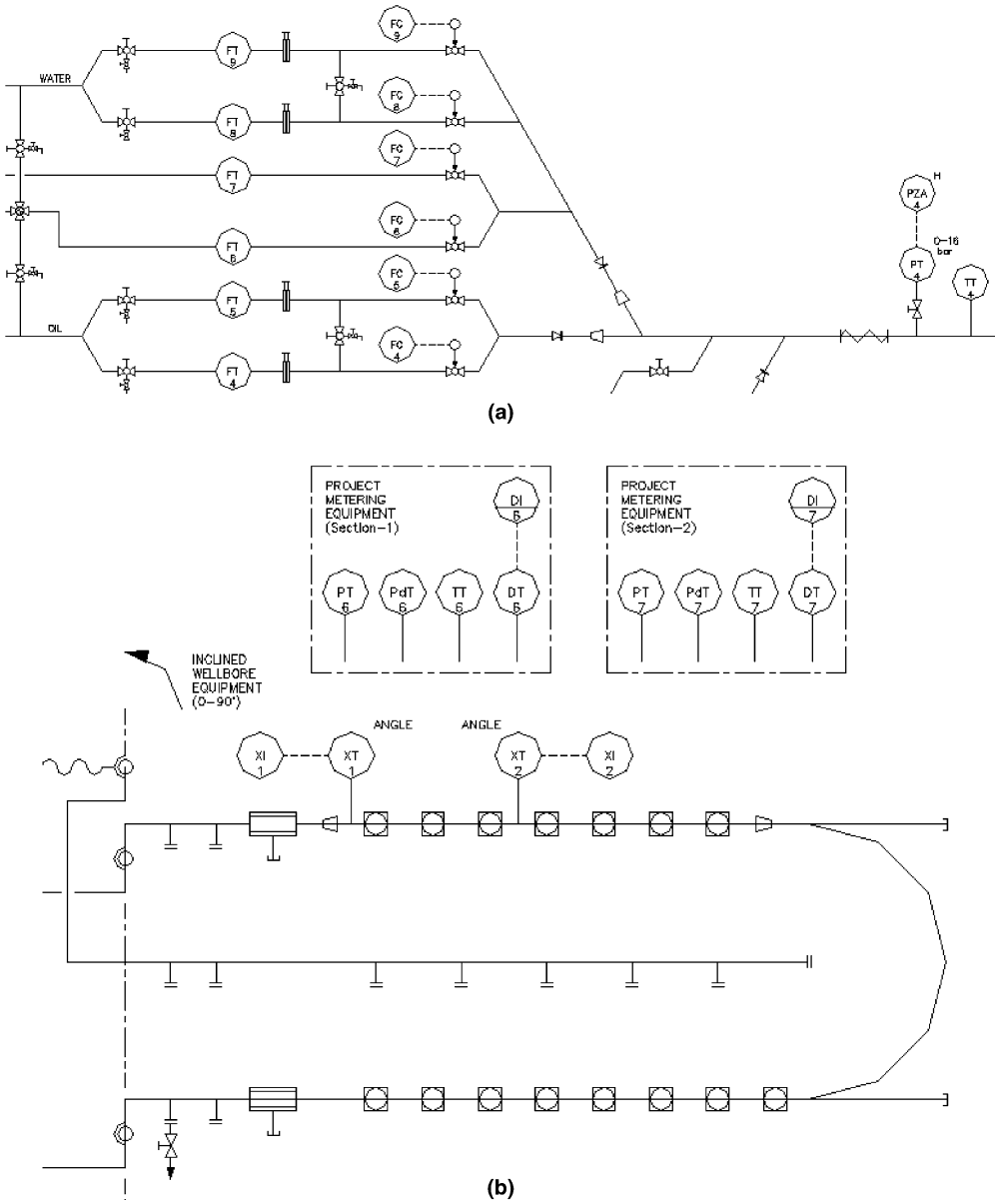

Fig. 1. Schematic view of the flow loop: (a) mixing section and (b) test section; FT single-phase density meter, FC flow meter, PT pressure meter, PdT differential-pressure meter, TT temperature meter, DT gamma densitometer.

flow, gas reaches the top of the separator and escapes through a chimney, while the liquid phases remain in the separator (Fig. 2). In this work there were only liquid phases, therefore the separation process was even more effective. The separator contains several 45°-oriented coalescent plates to accelerate the segregation of the liquid phases. Fig. 2 shows a schematic view of the separation process and storage of liquids.

2.3. Flow loop instrumentation

The instrumentation used in the experiments provided two types of data, the reference measurements of flow, deviation, density, pressure and temperature, and the detailed measurements required to determine the holdup and two-phase pressure gradient. Flow meters (Micro Motion, Coriolis elite massflow meters

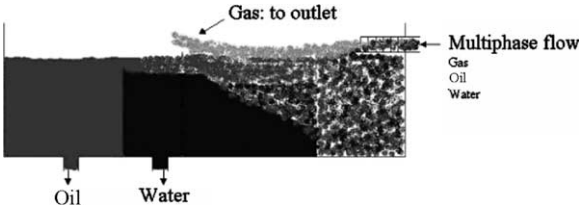

Fig. 2. Schematic view of the separation of oil, water and air, and storage of liquids inside the coalescent-plate separator; air (light gray), oil (dark gray) and water (black).

CMD 50/100/200), differential (one arm connected to a reference pressure line), gauge and absolute pressure meters (Rosemount 3051C), temperature meters (Metatemp Pt 100) and density meters (Schlumberger, Solartron 7835B) were part of the reference measurements instrumentation. Video recording (Sony digital video recorder DSR-20P, tapes Sony ME DVM60) was used for the flow patterns identification and gamma-ray densitometry (density meter Berthold LB 444) for the accurate measurement of the in situ volumetric fraction of the phases (holdup). Two independent computers were used to conduct the tests and to collect the data. A controller based on LabView® allowed to set the input water and oil flow rates and to select the appropriate pumps and flow meters. The second dedicated computer controlled the gamma densitometers.

Considering steady-state oil–water flow, a time-averaged symmetric distribution of the phases is expected if a vertical plane is taken in the axial direction intersecting the pipe diameter, regardless the flow pattern. In addition, no intermittent flow pattern, such as slug flow, is to be observed if the oil is relatively light (Trallero, 1995; Elseth, 2001; Bannwart et al., 2004). If we assume that the statements above are correct, an attenuation technique based on a constant acquisition time can be a reliable solution for liquid–liquid mixture density measurement. The chosen technique was the gamma-ray densitometry, which has been already successfully applied in oil–water flows (Elseth, 2001; Oddie et al., 2003). The gamma-ray densitometer measures the gamma beam absorption and allows the mean density of the mixture in the pipe to be calculated. One nuclear densitometer was installed at the beginning and another at the end of the inclinable test section to assess the full development of the two-phase flow, i.e., if the two-phase flow is fully developed, both devices should deliver the same mixture density value (no significant difference was detected). The devices were installed on the pipe with the gamma source making an angle of 45° with the vertical diameter, which aimed to better sampling. The same calibration procedure was carried out for each device. The pipe was first filled with water and data were gathered for 5 min giving typical counts. Afterwards, the pipe was filled with oil and the calibration procedure was repeated. With these count rates, the measured density of a pure fluid in the path of the gamma ray could be estimated to 0.82% accuracy. The mean density of the in situ mixture, ρ_m, is determined from the gamma densitometer count and the calibrations. In fully-dispersed flow or homogeneous flow, the water holdup (in situ volumetric fraction of water), $\varepsilon'_{w,hom}$, is calculated by

$$\varepsilon'_{w,hom} = \frac{\rho_m - \rho_o}{\rho_w - \rho_o}. \tag{1}$$

If we assume that the time and space-averaged mixture density supplied by the 45°-oriented gamma-beam device is a local quantity for the steady-state conditions studied, the water holdup can be directly correlated to the water height in fully-dispersed flow. However, for stratified flow a geometrical correction should be introduced to account for the phase distribution along the pipe curvature (Oddie et al., 2003). The water holdup for stratified flow, $\varepsilon'_{w,strat}$, is given by

$$\varepsilon'_{w,strat} = \frac{1}{\pi}\left\{\cos^{-1}\left(1 - 2\varepsilon'_{w,hom}\right) - \left(1 - 2\varepsilon'_{w,hom}\right)\sin\left[\cos^{-1}\left(1 - 2\varepsilon'_{w,hom}\right)\right]\right\}. \tag{2}$$

Here the homogeneous holdup (Eq. (1)) is used in the right-hand side of Eq. (2). The differences between $\varepsilon'_{w,strat}$ and $\varepsilon'_{w,hom}$ are relatively slight. The maximum relative differences were found at the lowest values of water holdup and were of the order of 7%. Therefore, although Eqs. (1) and (2) are valid for the extreme flow situations of complete mixing and complete phase separation, errors fairly below 7% are expected when applying Eqs. (1) and (2) to intermediate flow situations.

3. Test matrix

The main goal of the experimental work was to generate a comprehensive set of oil–water flow data, which would cover the entire range of flow rates and a significant range of deviations from horizontal. It should be possible to observe all flow patterns thus far reported in the literature and the characteristics of each one, at different inclinations. About 40 points were collected for each inclination (a point means a pair of oil and water superficial velocities or flow rates). The ranges of oil and water flow rates covered were 0.39–58.41 m^3/h and 0.31–48.54 m^3/h, respectively. The ranges of superficial velocities covered were $0.02 < U_{os}$ (oil) < 3.00 m/s and $0.02 < U_{ws}$ (water) < 2.55 m/s. Therefore, the mixture velocities varied from 0.04 m/s to 5.55 m/s. A graphical version of the test matrix for the seven pipe inclinations is shown in Fig. 7, which will be discussed in detail in Section 6. The total experimental data set consists of 296 points. In addition 14 tests were repeated, so the total number of tests conducted was 310.

4. Data sampling

The data collected in this work were found to follow a Gaussian distribution with time. The reference measurements, which include single-phase flow rates, densities of the phases, pressures and temperatures, presented an uncertainty of 0.1% of range. Two-phase pressure gradient measurements presented an uncertainty of about 1% of range for most of the experiments. Greater experimental uncertainties (of the order of 350% or even higher) were detected around $dp/dz = 0$. These data clearly were unsuitable for a proper analysis. Regarding the water holdup measurements, uncertainties of the order of 1% of range were computed for most of the experiments. Higher uncertainties of the order of 10% were detected for the lowest holdups.

Three measurements should be highlighted: frictional pressure drop, single phase viscosity and mixture density. In order to extract the frictional pressure-drop data from the measured overall pressure-drop data in the inclined flow tests, we used the measured holdup data to calculate the static pressure component. Single phase viscosity is an important quantity for the modeling of pressure gradient in both stratified and dispersed flows. However, it had to be determined indirectly since no in-line measurements of single phase viscosity were possible in the setup we used. Samples of oil and brine were collected during the tests, from which viscosity curves as a function of temperature were obtained (capillary viscometer, Schott-Geräte type AVS 310). Such analysis was carried out mainly in order to verify the possible stable incorporation of water into oil during the tests, which may increase significantly the oil viscosity. No change in viscosity along the tests was detected. On-line temperature data together with the experimental curve for the viscosity were subsequently used to determine the oil and water viscosity values for each experimental point. The on-line measured temperatures at which physical properties of fluids (density and viscosity) were measured ranged from 35.4 to 50.5 °C for water and from 37.5 to 53.9 °C for oil.

The only detailed measurement that was not obtained via the acquisition software was the mixture density. As described above, the gamma densitometer had its own dedicated computer for the acquisition and treatment of the data. The assumption of no-slip was used to determine the experimental uncertainties related to the gamma-ray densitometry. If we have a homogeneous flow, the mixture density can be given by the homogeneous model (Wallis, 1969):

$$\rho_{m,hom} = \rho_w \varepsilon_{w,hom} + (1 - \varepsilon_{w,hom})\rho_o. \tag{3}$$

In which

$$\varepsilon_{w,hom} = \frac{U_{ws}}{U_{ws} + U_{os}}. \tag{4}$$

Here U_{xs} stands for the superficial velocities. Such homogeneous flow was detected in our experiments at mixture velocities above 2 m/s ($U_m = U_{os} + U_{ws}$) and includes both oil-in-water (o/w) and water-in-oil (w/o) homogeneous dispersions. In Fig. 3 the mixture density provided by the gamma-ray densitometer, $\rho_{m,exp}$, is compared with the mixture density predicted by the homogeneous model, $\rho_{m,hom}$ (Eq. (3)), for the whole set of fully-dispersed flow data obtained, i.e., o/w and w/o flow patterns, including the horizontal and all inclined flows.

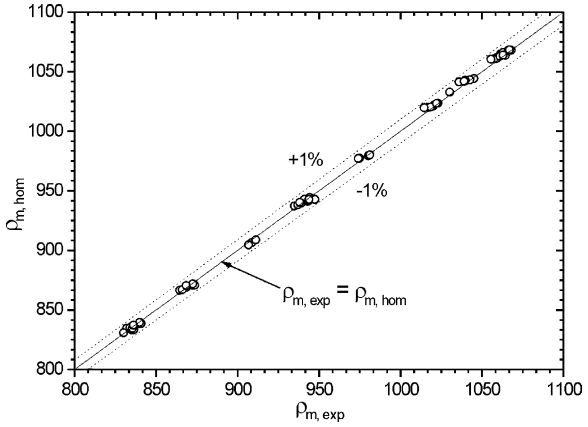

Fig. 3. Gamma-ray mixture density, $\rho_{m,exp}$, against homogeneous mixture density, $\rho_{m,hom}$, for the horizontal and all slightly inclined flows studied.

The figure illustrates that a good agreement could be achieved between the gamma-ray and the homogeneous mixture densities, with less than 1% of deviation. The results shown in Fig. 3 can be used to estimate the accuracy of the mixture density data (1%) if one assumes that for the fully-dispersed flow observed in these experiments the homogeneous model truly represents the distribution of the phases.

5. Holdup and pressure gradient models

The models applied for holdup and pressure gradient calculations are the area-averaged steady-state one-dimensional two-fluid model for stratified flow and the homogeneous model for dispersed flow. Although these are valid for the extreme flow situations of complete phase separation (i.e., without entrainment) and complete mixing, respectively, the comparison are thought to provide valuable guidelines on the applicability and prediction accuracies when these simple models are used for intermediate flow configurations as well.

In the two-fluid model the flow parameters (actual velocities, holdup, etc.) are calculated from the combined momentum equation for steady-state flow. Thus, eliminating the pressure drop from the equations of each phase:

$$-\frac{\tau_w S_w}{A_w}+\frac{\tau_o S_o}{A_o}\pm\tau_i S_i\left(\frac{1}{A_w}+\frac{1}{A_o}\right)-(\rho_w-\rho_o)g\sin\theta=0. \tag{5}$$

Here τ_x stands for the shear stress, S_x the wetted perimeter, A_x the cross sectional area, ρ_x the density and θ the inclination angle from the horizontal. The upper sign of the interfacial-stress term corresponds to the upper phase (oil) flowing faster than the bottom phase (water). Eq. (5) is a non-linear equation which can be solved for the liquid level or holdup using a standard numerical method if the shear stresses are expressed in terms of known friction factors. Additional relationships are required for calculating the geometrical variables (A_o, A_w, S_o, S_w and S_i as a function of holdup) and they can be found in Trallero (1995) or Fairuzov (2001). Closure relationships required for shear stresses in Eq. (5) are summarized in Appendix A. The pressure gradient is subsequently found by inserting the calculated holdup values into the one-dimensional differential equations of momentum for oil or water.

The homogeneous model for the pressure gradient in a liquid–liquid dispersion is often given as

$$\frac{dp}{dx}=-\frac{f_{m,hom}\rho_{m,hom}U_m^2}{2D}-\rho_{m,hom}g\sin\theta. \tag{6}$$

Here $f_{m,hom}$ is the mixture friction factor, $\rho_{m,hom}$ is the mixture density, U_m is the mixture velocity and D the pipe's internal diameter. The mixture parameters are basically treated as holdup-weighted relations (Eqs. (3) and (4)). Since this work was not concerned about phase inversion, the mixture viscosity, $f_{m,hom}=f(\mu_m)$, was simply treated using the homogeneous relation as presented in Elseth (2001). There are concerns on the

applicability of the homogeneous model in view of expected heterogeneous phase distribution due to segregation effects by gravity. The performance of the models described above has been recently tested against data from literature for oil–water horizontal flows (Rodriguez et al., 2004).

6. Experimental results and model comparisons

6.1. Flow patterns

The oil–water flow patterns observed in this work are in line with the flow pattern classification proposed by Trallero (1995). The only difference is the stratified wavy (SW) flow pattern observed in downward and upward flow. SW does not present any mixing at the interface and in the flow map is located between the stratified smooth (ST) and the stratified with mixing at the interface (ST&MI) flow patterns (Table 2).

The stratified and semi-stratified flow patterns: ST, SW, ST&MI and Do/w&w, and the oil-in-water homogeneous dispersion (o/w) could be characterized by watching the recorded movies of the flow. However, due to speed and resolution limitations of the video recording system, it was not possible to distinguish between the water-in-oil homogeneous dispersion (w/o) and a possible Dw/o&Do/w flow pattern in the oil-dominated region (in this text the term oil-dominated indicates the region of highest oil flow rates and lowest water flow rates, it does not mean necessarily an oil-continuous region; similarly for the term water-dominated). Both flow patterns were expected to occur according to some authors (Trallero, 1995; Alkaya et al., 2000; Elseth, 2001; Lovick and Angeli, 2004).

Photographs of the flow patterns are shown in Fig. 4 (all pictures correspond to horizontal flow, with the exception of the picture related to the SW flow pattern, which corresponds to downward flow). Note that the same picture is shown for both w/o and Dw/o&Do/w flow patterns, in accordance to what was mentioned above. With respect to the Stratified Wavy (SW) flow pattern, its most remarkable hydrodynamic feature is the stable wavy structure of the interface. No sign of dispersion at the interface was observed whatsoever.

Table 2
Flow patterns observed

Stratified smooth	ST
Stratified wavy	SW
Stratified flow with mixing at the interface	ST&MI
Dispersion of oil in water and water	Do/w&w
Oil in water homogeneous dispersion	o/w
Water in oil homogeneous dispersion	w/o
Dispersions of water in oil and oil in water	Dw/o&Do/w

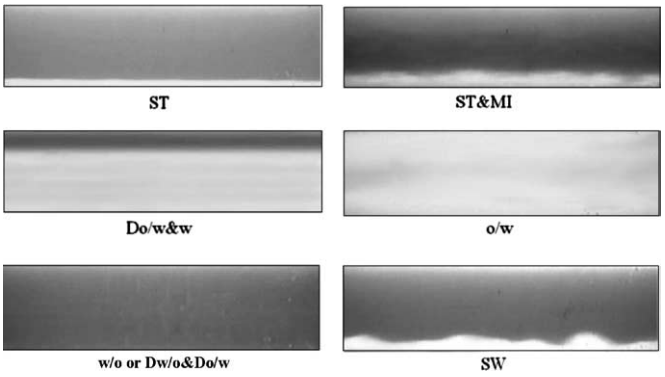

Fig. 4. Pictures of the flow patterns observed in this work (snap shots taken from the recorded movies; white is water; light gray is oil and dark gray is dispersion).

The SW flow pattern was clearly observed in downward flow. In the downhill flows studied (−1.5°, −2° and −5°) the SW flow pattern seemed to be systematically located in between the stratified Smooth (ST) and the Stratified with Mixing at the Interface (ST&MI) flow pattern regions. On the other hand, in the upward flows studied the SW pattern was also seen, but in a different region of the flow map. A stable wavy structure resembling a caterpillar was visible at low water and medium oil superficial velocities. Such caterpillar waves (Fig. 5) seemed to occur due to a combined effect of water backflow, detected at the bottom of the pipe, and water recirculation near the interface. The water backflow and recirculation phenomenon (Fig. 7g) could be visually observed through small oil droplets which would be carried along the relative water flow enclosed in between the bottom of the pipe and the oil–water interface. Finally, wavy structures were in fact also observed in horizontal flow; however, then there were always traces of mixing at the interface.

We have investigated whether there would be a dual-continuous Dw/o&Do/w flow pattern in the oil-dominated region (Lovick and Angeli, 2004). For that purpose we applied the homogeneous model. Assuming that the homogeneous model represents very well the phases distribution for fully-dispersed flow patterns, it should be possible to detect a relative deviation from the homogeneous behavior by comparing the holdup results of the w/o flow pattern with the results of the Dw/o&Do/w flow pattern. The relative deviation from the homogeneous behavior was quantified by comparing the experimental water holdup to that predicted by the homogeneous model as follows:

$$100 \cdot \left(\frac{\varepsilon_{w,hom} - \varepsilon_{w,exp}}{\varepsilon_{w,exp}} \right) = \% \text{ of deviation from homogeneous behavior.} \tag{7}$$

Fig. 6 shows the relative deviation from the homogeneous behavior as a function of water superficial velocity for a constant oil superficial velocity ($U_{os} = 3.00$ m/s) in horizontal and +2°-inclined flow. In horizontal flow (Fig. 6a) one may see that the two flow patterns behave rather similar, both not deviating much more than 1% from the homogeneous, no-slip, model. A different behavior is seen for one of the data for the dispersion of water in oil and oil in water (Dw/o&Do/w) for the 2°-upward flow. At a water superficial velocity $U_{ws} = 1.40$ m/s the change of trend is rather clear (Fig. 6b, about 10% deviation). What is in fact clearly observed in Fig. 6 is the systematic increase of the deviation from the homogeneous behavior with the increase of the water superficial velocity. However, at the highest water superficial velocities the trend is inverted. Such inversion of trend may actually denote phase inversion from oil-continuous to water-continuous flow. Therefore, the detected change of trend and the relatively higher deviation from the homogeneous behavior could be considered as possible evidences of the existence of the dual-continuous Dw/o&Do/w flow pattern region. Analogous results were obtained for the other inclinations.

Fig. 7 shows the entire set of experimental flow maps for horizontal and slightly inclined flows (symbols) together with the predictions of the flow pattern model (solid lines). The agreement between the experimental flow map and that predicted by the model was 80% or above for horizontal and downward flows (Fig. 7a–d). At this stage the SW flow pattern is still considered as a kind of ST&MI. The agreement reaches 95% if one considers the ST and ST&MI patterns as stratified flow patterns and the rest as dispersed. As a matter of fact, the ST&MI may correspond to a dual-continuous flow pattern (Lovick and Angeli, 2004), since significant dispersion at the interface was detected. However, the holdup evaluation (Section 6.2) shows that this flow pattern presents a slip behavior of a completely segregated phase distribution. Such apparently large differences happened basically at the stratified region. Considering the horizontal flow (Fig. 7a), one may notice that the model overestimates the ST region. That disagreement had been already observed from a comparison

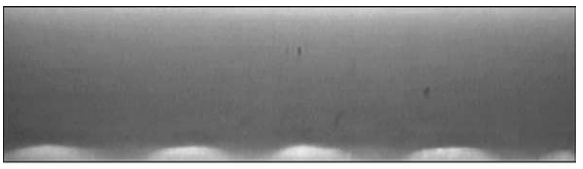

Fig. 5. Caterpillar waves.

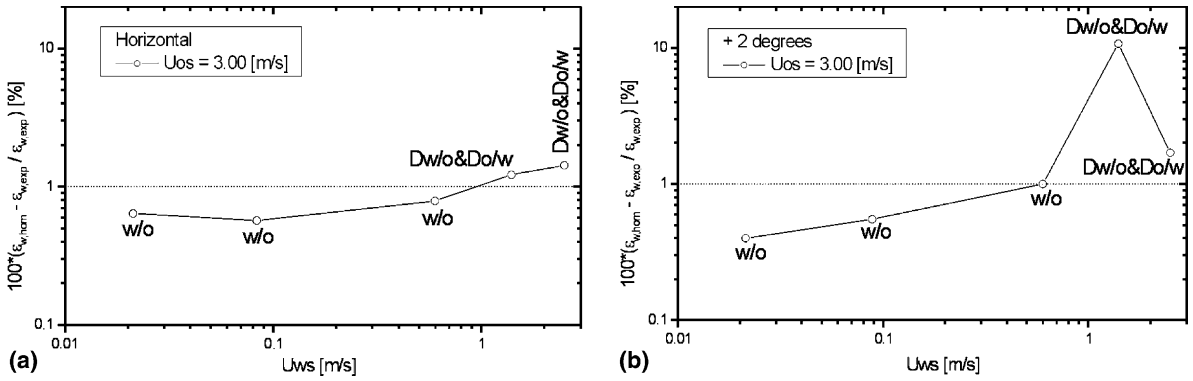

Fig. 6. Relative deviation from the homogeneous behavior in the oil-dominated region: (a) horizontal flow and (b) +2° inclined flow; 1%-deviation dotted line shown as reference purposes only.

with data from the literature (Rodriguez et al., 2004). Such a result suggests that the stability-analysis transition criteria for stratified flow require further improvement, especially when applied to larger diameters. On the other hand, the ST&MI boundary works quite well (Fig. 7a): the predicted and experimental ST&MI transition boundaries almost match. A slightly worse agreement was obtained for upward flow, 75% or above (Fig. 7e–g). The higher disagreement in this case was due to the split of the predicted ST region into two new ST regions, with no apparent physical meaning. If one considers the ST and ST&MI as stratified flow patterns and the rest as dispersed the agreement also reaches 95%. Such overall agreement is of the same order as that presented by the latest mechanistic models found in the literature (Petalas and Aziz, 2000).

With respect to the inclination angle effect on flow patterns, in downward flow the ST pattern tends to disappear. The ST region was somewhat substituted by the SW pattern. Another remark regards the Do/w&w region, which tends to increase with downward inclination towards the ST&MI region (Fig. 7d). In upward flow the ST pattern also tends to disappear. The new wavy flow pattern SW—caterpillar wave was detected at low water and mid oil superficial velocities (Fig. 7f). In the highest upward inclination the SW pattern also disappeared and a region of strong water backflow and recirculation was detected at low water and mid oil superficial velocities (Fig. 7g).

A last remark should be made regarding the new sub-region predicted in the 5°-uphill flow (Fig. 7g). The new ST&MI* sub-region observed in the ST&MI region, at medium/low water and medium oil superficial velocities, was actually predicted by the model as an o/w homogeneous dispersion region. The experimental points related to this area are those for which strong water backflow at the bottom of the pipe and water recirculation at the interface were observed.

6.2. Holdup

We will now compare the water-holdup data first qualitatively and then quantitatively with predictions of the two-fluid model for stratified flow and the homogeneous model for dispersed flow. It is important to point out that the global holdup predictions depend on the flow-pattern model. Therefore, the choice for a suitable holdup model can only be made after the definition of which flow pattern behaves as stratified or dispersed flow. Unfortunately, the choice is not trivial, especially for the case of dual-continuous flows. Dual-continuous flows are somewhat between the stratified and fully-dispersed flows in terms of the in situ distribution of the phases (Lovick and Angeli, 2004). We present the holdup results as function of the water superficial velocity for a constant oil superficial velocity. Six different oil superficial velocities (0.02, 0.07, 0.30, 0.60, 1.50 and 3.00 m/s), spanning all flow map regions, have been analyzed.

Fig. 8 shows for two of the oil superficial velocities investigated, 0.30 and 1.50 m/s, comparisons between horizontal-flow data and results calculated with the two-fluid model (drawn curve) and the homogeneous model (dotted line) as a function of the water superficial velocities. The comparison is made via the (water cut)/(water holdup) ratio, C_w/ε_w, which gives a suitable relative representation of the liquid–liquid slip or

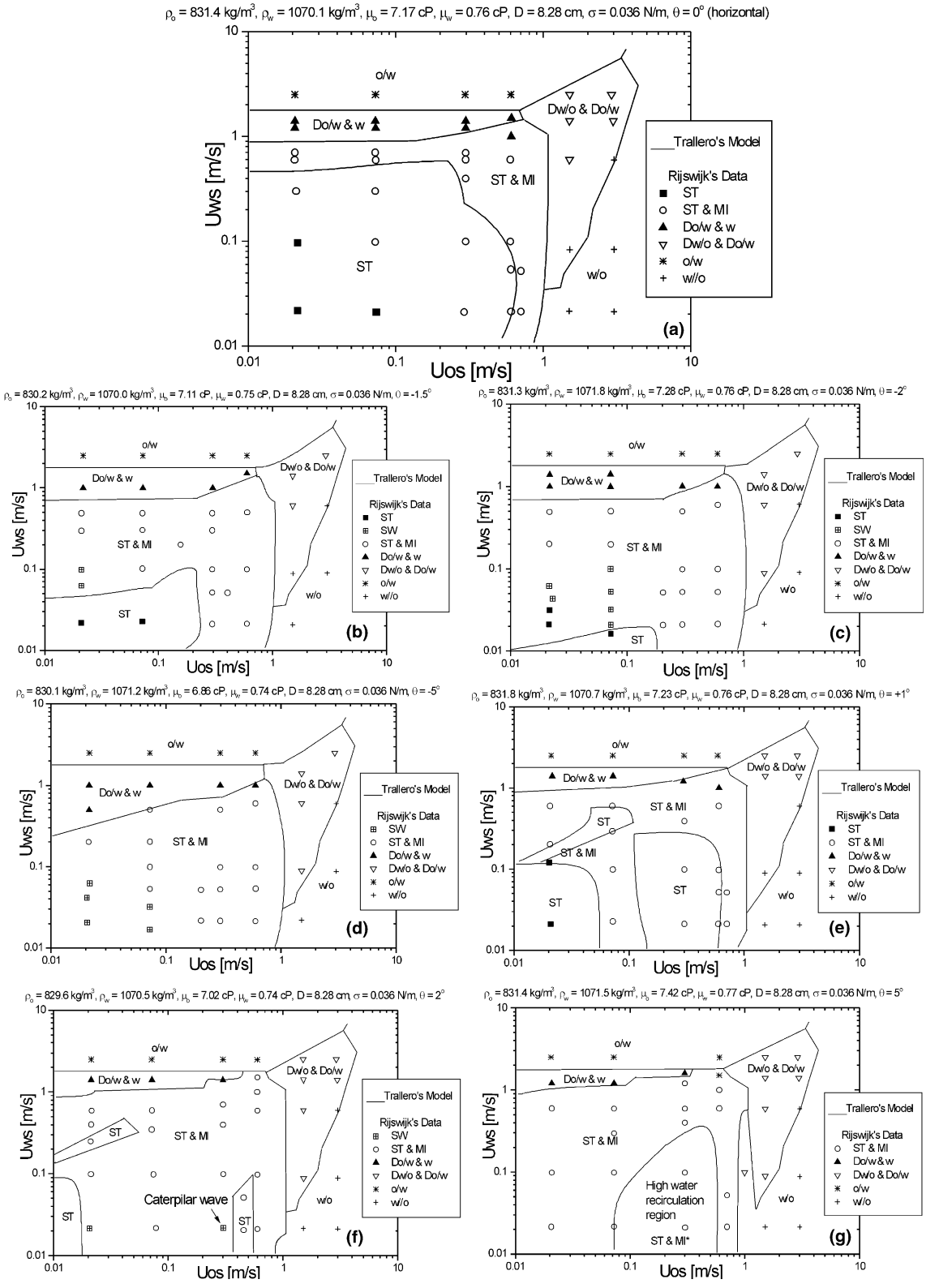

Fig. 7. Experimental (dots) and predicted (solid lines) flow pattern maps: (a) horizontal flow, (b) −1.5°, (c) −2°, (d) −5°, (e) 1°, (f) 2° and (g) 5°.

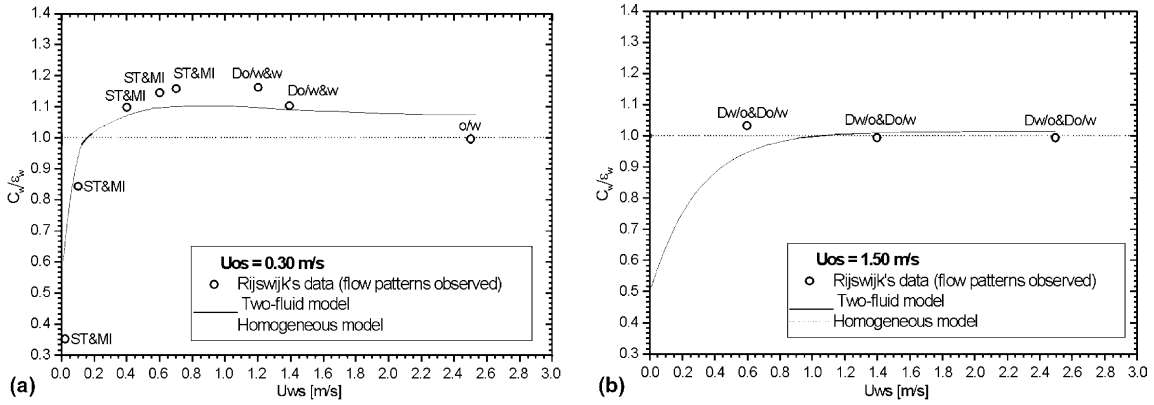

Fig. 8. C_w/ε_w in horizontal flow as a function of the water superficial velocity; experimental results (dots), two-fluid model (solid line) and homogeneous model (dotted line); (a) $U_{os} = 0.30$ m/s and (b) 1.50 m/s.

in situ phase accumulation. By inspection of Fig. 8 one may see that the two-fluid model (solid line) agrees reasonably well with the trend presented by the experimentally obtained ST&MI and Do/w&w dots (refer also to Table 2). The dots related to o/w and Dw/o&Do/w flow patterns are more in line with the homogeneous model (dotted line).

In upward flow there is an expected trend of in situ accumulation of the denser phase, in this case water. Hence, the C_w/ε_w ratio is expected to reach lower values in comparison to horizontal flow. Fig. 9 shows for a pipe angle of $+5°$ the comparisons of measurements and model calculations for two of the oil superficial velocities studied, 0.30 and 1.50 m/s. The two-fluid model (solid line) and the homogeneous model (dotted line) reasonably well represent the trend of the experimental points related to stratified (ST&MI) and oil-dominated dual-continuous (Dw/o&Do/w) flow patterns.

For downward flow there is an expected trend of in situ accumulation of the lighter phase (in this case oil). Hence, the C_w/ε_w ratio is expected to reach higher values compared to horizontal and upward flow. Fig. 10 shows the results for a pipe angle of $-5°$ and oil superficial velocities of 0.30 and 1.50 m/s. The two-fluid model (solid line) agrees reasonably well with the experimentally obtained ST&MI and Do/w&w, and the homogeneous model (dotted line) with the data related to the fully dispersed o/w. Some ambiguity is observed for the oil-dominated dual-continuous Dw/o&Do/w flow pattern. At low water superficial velocities the two-fluid model seems to be better. However, at high velocities, which represented most cases studied, the homogeneous model presents better results.

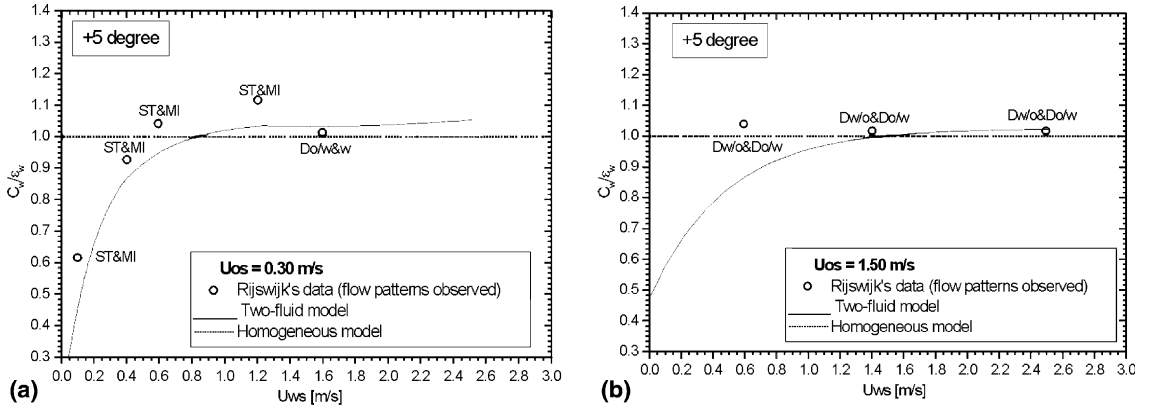

Fig. 9. C_w/ε_w in 5°-upward flow as a function of the water superficial velocity; experimental results (dots), two-fluid model (solid line) and homogeneous model (dotted line); (a) $U_{os} = 0.30$ m/s and (b) 1.50 m/s.

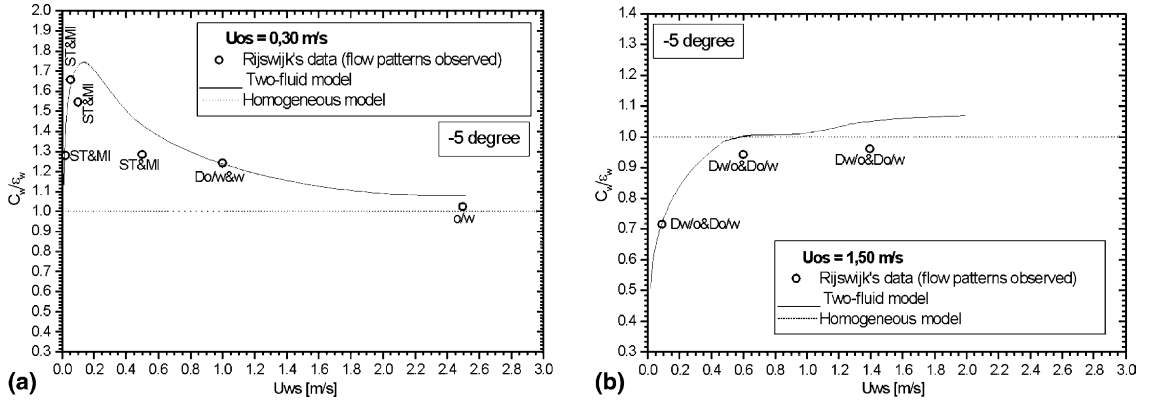

Fig. 10. C_w/ε_w in $-5°$-downward flow as a function of the water superficial velocity; experimental results (dots), two-fluid model (solid line) and homogeneous model (dotted line); (a) $U_{os} = 0.30$ m/s and (b) 1.50 m/s.

We can summarize the above analysis of the holdup models by observing that the two-fluid model should be applied to the ST and ST&MI flow patterns, whereas the homogeneous model should be applied to the o/w and w/o. On the other hand, it is not perfectly clear which model should be applied to the water-dominated Do/w&w flow pattern and oil-dominated Dw/o&Do/w dual-continuous flow pattern. Nevertheless, most of the experimental data confirm the homogeneous model as a more adequate holdup model for the Do/w&w and Dw/o&Do/w flow patterns.

The effect of deviation from the horizontal is now qualitatively analyzed for uphill and downhill flows. Such effect, predicted by the two-fluid model, is compared with the data. Fig. 11 shows the (water cut)/(water holdup) ratio, C_w/ε_w, as a function of the uphill inclination angle. Although there is a relatively significant deviation from the two-fluid model curves, the data (Fig. 11, dots) present the same trend of moving towards lower C_w/ε_w values by increasing the uphill inclination angle. Fig. 12 shows C_w/ε_w as a function of the downhill inclination angle. Also here the data present the same trend as the two-fluid model: now moving towards higher C_w/ε_w values when the angle becomes steeper, as expected. Note that in Figs. 11 and 12 the two-fluid curves for the low oil velocity case approach the homogeneous model results at higher water velocities, whereas for the 0.30 m/s oil velocity case (Figs. 11b and 12b) the two-fluid results asymptote to a value that is consistently higher than the no-slip values.

The results of the holdup models (two-fluid model and homogeneous model applied to their respective flow patterns) are now quantitatively compared with our data. The values predicted by the models are compared with the experimental data by using the average relative error (e):

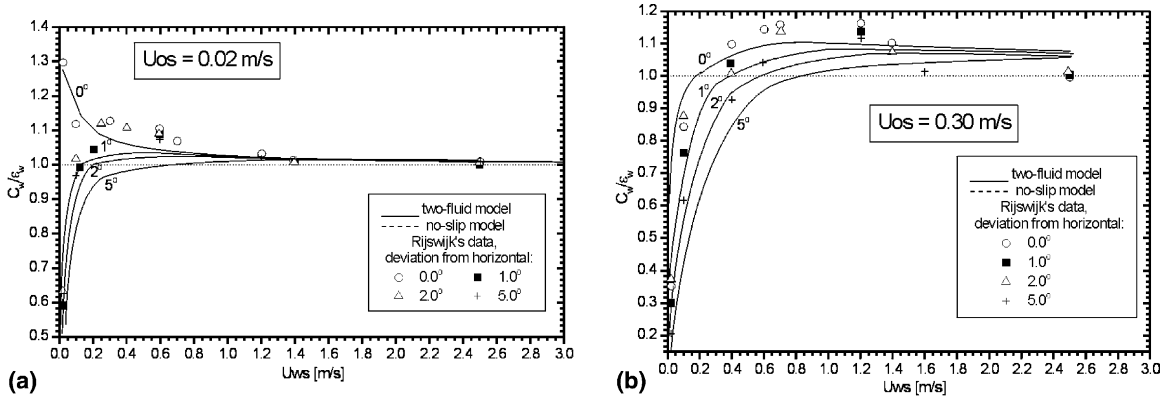

Fig. 11. C_w/ε_w, as a function of the uphill inclination angle; experimental results (dots), two-fluid model (solid line) and homogeneous model (dotted line); (a) $U_{os} = 0.02$ m/s and (b) 0.30 m/s.

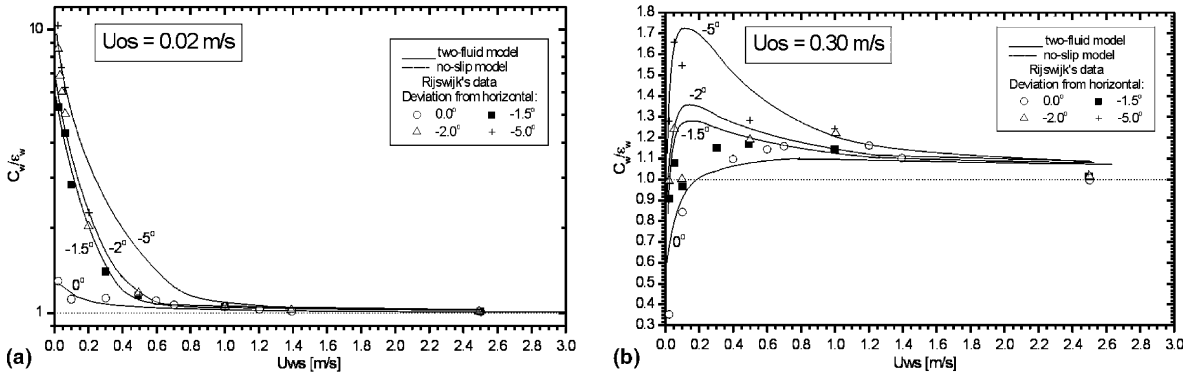

Fig. 12. C_w/ε_w, as a function of the downhill inclination angle; experimental results (dots), two-fluid model (solid line) and homogeneous model (dotted line); (a) $U_{os} = 0.02$ m/s and (b) 0.30 m/s.

$$e = 100\frac{\sum_N \sqrt{\left(\frac{f_{FP}[(k_{mod})_{2f},(k_{mod})_{hom}]-k_{exp}}{k_{exp}}\right)^2}}{N}[\%]\ . \tag{8}$$

Here f_{FP} denotes a functional relation with flow pattern, k is either holdup or pressure gradient, the subscript mod indicates model prediction (2f two-fluid model and hom homogeneous model) and the subscript exp the respective experimental point; N is the number of runs carried out. In addition, the maximum deviation (dev) of the points (spreading) gives an impression of the accuracy of the models. Although such analysis includes both systematic and random experimental errors, in most of the cases the observed spreading is mainly due to imperfections of the models (refer to Section 4). Only for pressure gradients around zero the experimental uncertainties may have superseded the model errors. Table 3 shows a comparison of experimental data and predicted water holdup as a function of flow pattern and inclination. In this table the two-fluid model has been used for ST and ST&MI patterns and the homogeneous model for the others.

When we consider the survey of average relative errors and deviations large values are seen for the water-in-oil homogeneous dispersion, w/o. The best agreement was observed for the other dispersed flow patterns. Nevertheless, the accuracy of 15% offered by the two-fluid model is also reasonably good. Slightly worse accuracies of 25% are achieved for the downward-flow case. One may see that the two-fluid model and the homogeneous model tend to overestimate the water holdup in the ST&MI flow pattern for upward flow and in the Do/w&w flow pattern for horizontal and upward flow, respectively. On the other hand, the homogeneous model underestimates the water holdup in the Dw/o&Do/w pattern for downward flow. The relatively poor accuracies for w/o flow pattern are for a region of very low water holdups (always below 0.1) with relatively high experimental uncertainties.

In order to avoid any misinterpretation due to experimental uncertainties, regarding the overall comparison between the models and experimental data, the further analysis was carried out for water holdup values above

Table 3
Comparison of experimental data and predicted water holdup as a function of flow patterns and inclination

	0° inclination		+5°		−5°	
	e (%)	dev (%)	e (%)	dev (%)	e (%)	dev (%)
ST	13	±15	–	–	–	–
ST&MI	6	±15	9	+15	16	±25
Do/w&w	6	+15	4	+10	17	±25
o/w	1	±1	2	±5	2	+2
w/o	25[a]	−25[a]	15[a]	±20[a]	9[a]	±15[a]
Dw/o&Do/w	4	±5	7	±10	9	−15

SW is considered as a kind of ST&MI.
[a] Observed for water holdups lower than 0.1.

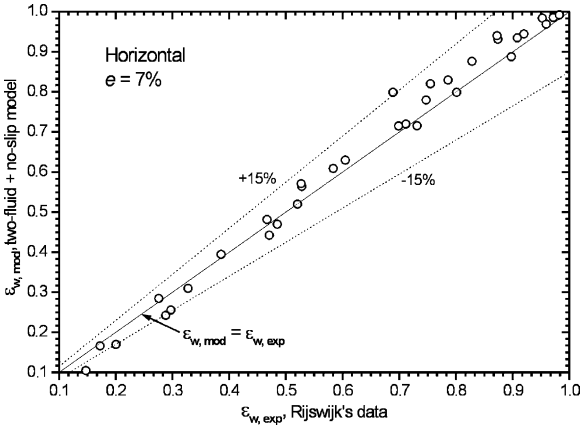

Fig. 13. In situ water holdup predicted by the models against in situ water holdup experimentally obtained; horizontal flow.

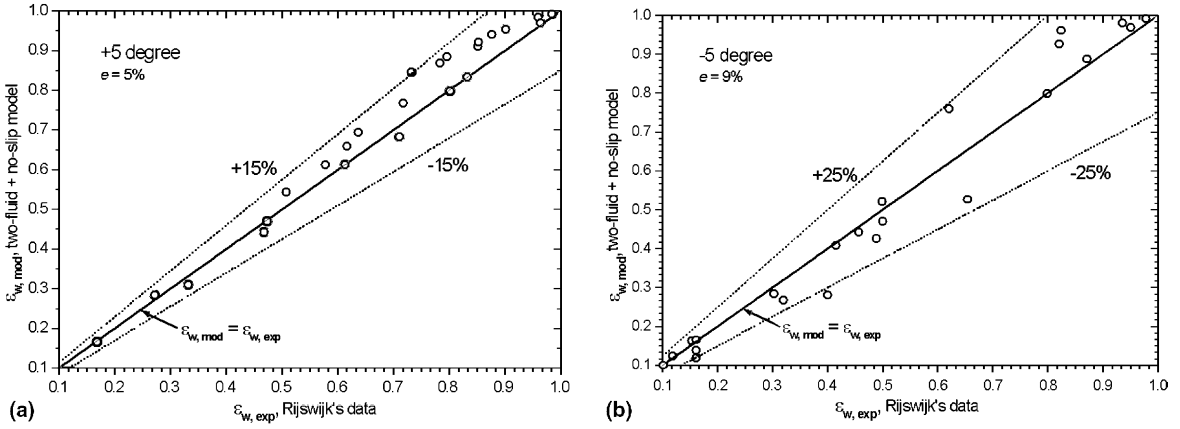

Fig. 14. In situ water holdup predicted by the models against in situ water holdup experimentally obtained: (a) upward flow, +5° and (b) downward flow, −5°.

0.1 only. As may be seen in Fig. 13, in horizontal flow the relative error is 7%, whereas the accuracy (or maximum deviation) is 15%. The same quantitative evaluation was carried out for upward and downward flow. Fig. 14 shows the comparison between the predicted and experimental water holdups. The calculation for a pipe angle of +5° (Fig. 14a), represented by an overall relative error of around 5% and an accuracy (or maximum deviation) of 15%, is relatively good. Fig. 14b shows a relatively poor agreement for −5°-downward flow. The overall relative error of the data is around 10%, whereas the accuracy (or maximum deviation) is of 25%.

6.3. Pressure gradient

The oil/water pressure-gradient data were also qualitatively and quantitatively compared with predictions of the two-fluid model for stratified flow and the homogeneous model for dispersed flow. The pressure gradient prediction also depends on the flow-pattern prediction model. In addition, its accuracy depends on the correct choice of the holdup model. Therefore, a pressure gradient model can only be applied after the definition of which flow pattern behaves as stratified or dispersed flow, i.e., after the choice of the adequate holdup model. According to the results presented above, the two-fluid model was applied to the ST and ST&MI flow patterns, whereas the homogeneous model was applied to the o/w, w/o, Do/w&w and Dw/o&Do/w flow patterns.

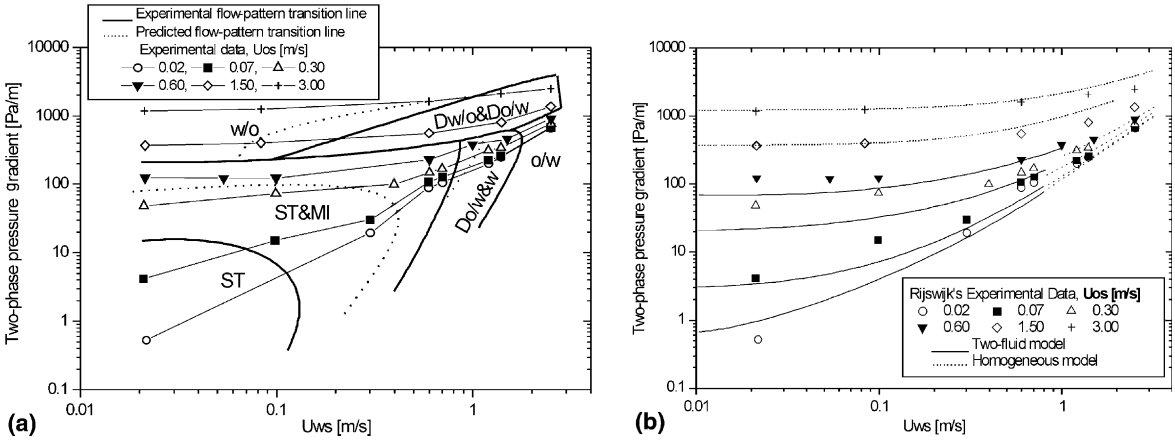

Fig. 15. Horizontal-flow oil–water pressure gradient as a function of the water superficial velocity for several constant oil superficial velocities: (a) experimental data (dots), experimental transition boundaries (solid lines) and model transition boundaries (dotted lines); (b) two-fluid model (solid lines) and homogeneous model (dotted lines).

Fig. 15 shows the horizontal-flow oil–water pressure gradient as a function of the water superficial velocity for several constant oil superficial velocities. The experimentally defined flow pattern regions (Fig. 15a, solid lines; from video data and analysis of deviation from homogeneous behavior) and the flow pattern transition boundaries predicted by the model (Fig. 15a, dotted line) are also shown as reference. Here once more it is clear that the ST transition boundary is responsible for the largest difference between predicted and observed flow pattern transitions (refer to Section 6.1). The transition from stratified to dispersed flow seems to happen somewhere in between the predicted ST-ST&MI transition boundary (dotted line; refer also to Fig. 7a) and the experimental ST&MI-Do/w&w transition boundary (solid line). The observed change of trend of the experimental data supports this statement. Such result reassures the right choice of treating the Do/w&w flow pattern as dispersed. Fig. 15b compares horizontal-flow data with models. The two-fluid model (solid lines) tends to underestimate the experimental points related to the stratified region (refer also to Fig. 15a), especially at the lowest water superficial velocities. However, the general trend is reasonably well predicted. The homogeneous model is doing a better job when comparing with experimental points related to the dispersed region (Fig. 15b, dotted lines; refer also to Fig. 15a). A larger mismatch between the homogeneous model and the respective experimental data points was observed only at the highest water and oil superficial velocities, where the model tends to overestimate the experimental data. The general trend is again reasonably well predicted. Elseth (2001) observed that in general the pressure-drop data fit the two-fluid model best for intermediate water-cuts, whereas for high water-cuts the model under-predicts the pressure drop. We find the same in Fig. 15b at water–oil volume ratios close to unity and at high water–oil ratios, respectively. Besides, we have found that at low water–oil ratios (or low water-cuts) the two-fluid model also under-predicts the pressure drop. Elseth (2001) also states that for dispersed flows the homogeneous model over-predicts at low water-cuts and under-predicts at high water-cuts. In Fig. 15b we may see that at high water–oil ratios (or high water-cuts) the homogeneous model slightly under-predicts the data, in accordance with Elseth's observations. However, for the low water–oil ratios (or low water-cuts) studied in this work we obtained the best agreement with the homogeneous model. On the other hand, in Fig. 15b the homogeneous model over-predicts the pressure gradient at water–oil ratios close to unity (or intermediate water-cuts).

Lovick and Angeli (2004) state that the standard two-fluid model is unable to predict the pressure gradient during dual-continuous flow. According to the flow pattern classification proposed in this work, ST&MI and Dw/o&Do/w flow patterns might be considered as dual-continuous flows, since they present features of both purely stratified and fully-dispersed patterns (Lovick and Angeli, 2004). The water-continuous Do/w&w flow pattern also presents features of both stratified and dispersed patterns. In this work the ST&MI was simply treated as stratified pattern and modeled by the two-fluid model. As one may notice by referring to Fig. 15, in the ST&MI region the two-fluid model predicts the pressure gradient with relatively good accuracy

at intermediate and high water–oil ratios. Relatively poor agreement is seen at low water–oil ratios. On the other hand, the Do/w&w and Dw/o&Do/w were simply treated as fully-dispersed patterns and modeled by the homogeneous model. In the Do/w&w region the agreement between the homogeneous model and pressure-gradient data is rather good, while in the Dw/o&Do/w region the homogeneous model overestimates the data (Fig. 15). Nevertheless, the agreement is also relatively good.

The models definitely could be improved by better predicting the transition from ST to ST&MI, the pressure gradient in the ST&MI at low water–oil ratios and the pressure gradient in the Dw/o&Do/w region at water–oil ratios close to unity. However, on the whole the simple models reasonably well reflect the trends of the pressure gradient for all flow patterns, including the dual-continuous flows.

Finally, model predictions are quantitatively compared with the experimental data through the average relative error (Eq. (8)) and the deviation. Table 4 shows a comparison of experimental data and predicted pressure gradients as function of flow pattern and inclination. In Table 4 the two-fluid model has been used for ST and ST&MI patterns and the homogeneous model for the rest. At a first glace, one may notice that poor accuracies are obtained in the ST flow pattern for horizontal flow and in the o/w and Dw/o&Do/w flow patterns for downward flow. At this region of $dp/dz \cong 0$ the data suffer from high experimental uncertainties. In horizontal flow, the models tend to underestimate the pressure gradient in the ST&MI and Do/w&w. In upward flow, the homogeneous model underestimates the pressure gradient in the Do/w&w flow pattern. On the other hand, the homogeneous model overestimates the pressure gradient in the Dw/o&Do/w flow pattern. In downward flow, the two-fluid model overestimates the pressure gradient in the ST&MI pattern and the homogeneous model overestimates the pressure gradient in the w/o flow pattern.

Fig. 16 shows an overall comparison of the pressure gradients predicted by the models and those experimentally obtained in horizontal flow. The two-fluid model underestimates the data at the lowest mixture velocities, whereas the homogeneous model tends to overestimate the data at the highest mixture velocities. These

Table 4
Comparison of experimental data and predicted pressure gradient as a function of flow patterns and inclination

	0° inclination		+5°		−5°	
	e (%)	dev (%)	e (%)	dev (%)	e (%)	dev (%)
ST	360[a]	500[a]	–	–	–	–
ST&MI	28	−35	10	±20	9	+15
Do/w&w	8	−20	6	−10	4	±5
o/w	4	+5 and −10	3	+2 and −5	67[a]	+100[a]
w/o	2	±5	2	±5	27	+35
Dw/o&Do/w	40	+35	18	+35	250[a]	+100[a]

SW is considered as a kind of ST&MI.
[a] Observed for pressure gradients around zero.

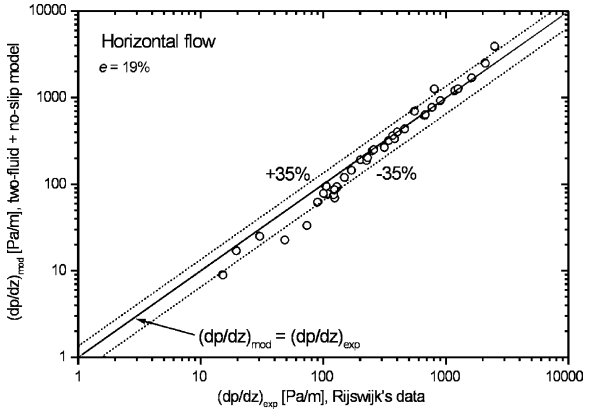

Fig. 16. Pressure gradients predicted by the models against pressure gradients experimentally obtained; horizontal flow.

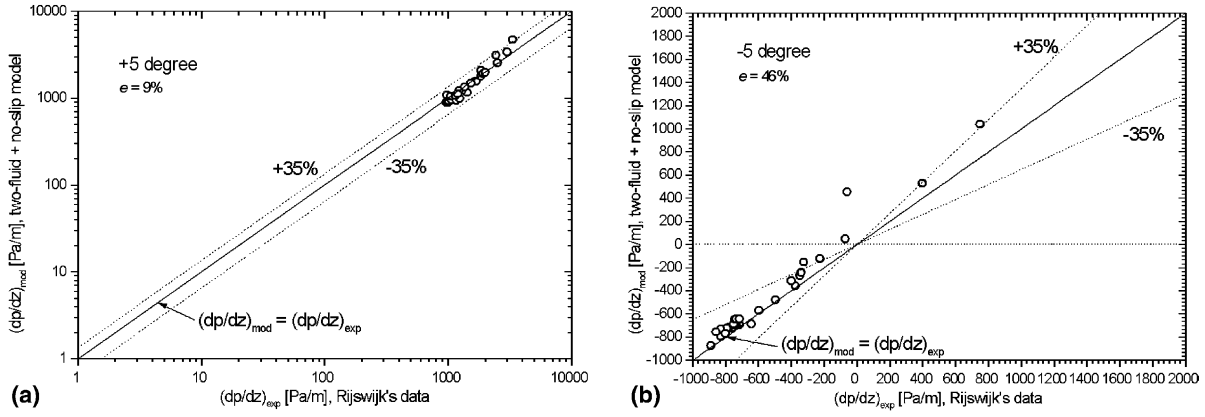

Fig. 17. Oil–water pressure gradient predicted by the models against oil–water pressure gradient experimentally obtained: (a) upward flow, +5° and (b) downward flow, −5°.

are responsible for the relatively high overall inaccuracy. Therefore, even though the relative error was found to be 19%, the accuracy (or maximum deviation) is as high as 35%.

The same quantitative evaluation was carried out for upward and downward flows. Fig. 17a compares for a pipe angle of +5° the predicted with the measured oil/water pressure gradients. The overall relative error is around 9% and the accuracy 35%. It can be also seen that the uphill inclination angle has an effect of increasing the pressure-gradient values, especially at the lowest mixture velocity points, as expected since for upward flow the frictional and gravitational pressure gradients are both against the flow. Notice that the relative error is slightly lower than that computed for horizontal flow. Apparently the gravitational term contributes to decrease the relative error between data and model predictions for some cases. Fig. 17b shows the comparison for a pipe angle of −5°. The evaluation took into account the region of negative pressure gradients, since in practice negative two-phase pressure-gradient values are to be acquired. The relative error ranged around 50%. Such relatively high error happened mainly due to the measurements taken around the "zero" value of pressure gradient. The experimental uncertainties around $dp/dz = 0$ were relatively high and are probably responsible for this. In general a more significant propagation of uncertainties may have happened, since in downward flow the holdup predictions were also relatively poor. As a matter of fact, the experimental uncertainties around $dp/dz = 0$ (Table 4) ruin any possible comparison between data and models. If such points are arbitrarily excluded from the error analysis the accuracy obtained is around 35%, which is similar to the horizontal and upward flow findings. Inclination affects mainly the lowest mixture velocity points, where gravity plays a more relevant role. Such points moved on towards lower pressure gradient regions with the increase of the downhill inclination angle, as expected since gravity now favours the flow.

We have to find out whether these relatively large errors lead to acceptable estimates of oil and water superficial velocities when we apply the inverse model technique. The results of the analysis can also serve as basis for further model developments. We have to realize that in the flow pattern dependent approach errors in flow pattern determination and in phase holdup both contribute to the relatively large errors in the oil/water pressure gradient predictions. So, attempts to reduce these sources of errors by model improvements should have a high priority. An omission is that we have not accounted for the possible occurrence of oil/water inversion, which may lead to increased frictional pressure losses at large mixture velocities and appropriate water-cuts. This aspect will be addresses in a forthcoming paper. Also, a more refined two-fluid model for dual-continuous flow patterns may improve the accuracy. This requires more refined measurements with proper information on drop entrainment, size and distribution in oil/water pipe flow. Such measurements are in preparation.

7. Conclusions

Flow patterns, phase holdups and pressure gradients have been measured for horizontal and inclined (−5°, −2°, −1.5°, 1°, 2° and 5°) oil/water flow in an 8.28 cm diameter steel pipe using mineral oil and brine as fluids

at mixture velocities from 0.04 m/s to 5.55 m/s. The measuring accuracies of water holdups varied from 0.1% to 10% (at water holdups lower than 0.1) of range and were of the order of 1% of range for most of the experiments. The measuring accuracies for oil/water pressure gradients were of the order of 1% of range for most of the experiments. The following main conclusions can be drawn from this experimental study:

- The seven observed oil–water flow patterns for horizontal, upward and downward inclined flow are reasonably well described by the Trallero's flow pattern map. For downward inclined flow a stable wavy structure was observed. For upward inclined flow regions with high water recirculation were detected. The stratified smooth flow pattern disappears with inclination and is replaced by a stratified wavy flow pattern.
- The measured holdup and pressure-gradient data have been compared with calculations using two simple models: the two-fluid model and the homogeneous model. Although these are valid for the extreme flow situations of complete phase separation (i.e., without entrainment) and complete mixing, respectively, the comparison provides valuable guidelines on the applicability and prediction accuracies when these models are used for intermediate flow configurations.
- With respect to the dual-continuous flows, the stratified flow pattern with mixing at the interface (ST&MI) presents slip behavior of a stratified flow, whereas the dispersions of water in oil and oil in water pattern (Dw/o&Do/w) behaves basically as dispersed flow. The dispersion of oil in water and water pattern (Do/w&w) presents an ambiguous behavior in terms of slip and might be treated as either stratified or dispersed flow.
- With these simple models prediction accuracies varied with flow pattern and pipe inclination. For horizontal flow prediction accuracies with the two-fluid model for water holdups are 15% for the stratified flow patterns (ST and ST&MI). With this model pressure gradients are predicted with accuracies of 35%. The homogeneous model performs best for the o/w and Dw/o&Do/w flow patterns with prediction accuracies for water holdup of 1% and 5%, respectively; its overall accuracy for the dispersed patterns was of 15%. With this model pressure gradients are predicted with accuracies of 35%. For upward flow similar results were obtained regarding the flow pattern effect. The prediction accuracies with the two-fluid model and the homogeneous model for water holdups are 15% and 10%, respectively. Oil/water pressure gradients are predicted by these models with accuracies of 20% and 35%, respectively. For downward flow the prediction accuracies with the two-fluid model and the homogeneous model for water holdups are both 25%. For pressure gradients they are 15% and 35%, respectively.

Acknowledgements

We are grateful to Shell International Exploration and Production B.V. for supporting this work. Sincere thanks are extended to Roel Kusters, Hans den Boer, Danny Kromjongh, and Arno van der Handel for the interesting discussions and their support in collecting the data on the DONAU flow loop, Rijswijk, The Netherlands. Oscar Rodriguez is grateful to Rob Mudde and Luis Portela for their continuous interest.

Appendix A. Closure relations for shear stress modeling

The wall shear stress acting on each phase is expressed in terms of the local velocity of the phase and corresponding friction factor. For the bottom phase, i.e., water:

$$\tau_w = f_w \frac{\rho_w U_w |U_w|}{8}, \tag{A.1}$$

where f_w is the water friction factor and U_w the local water velocity, and

$$f_w = \begin{cases} 64/Re_w = 64/(\rho_w D_{hw} U_w/\mu_w) & \text{for } Re_w \leqslant 1500 \\ \left\{-1.8\mathrm{Log}_{10}\left[\frac{6.9}{Re_w} + \left(\frac{e}{3.7D_{hw}}\right)^{1.1}\right]\right\}^{-2} & \text{for } Re_w > 1500, \end{cases} \tag{A.2}$$

where for transitional/turbulent flow the Haaland (1983) correlation is used, and Re_w is the water Reynolds number, D_{hw} is the water hydraulic diameter, μ_w is the water viscosity and e the pipe wall roughness. For the upper phase, i.e., oil:

$$\tau_o = f_o \frac{\rho_o U_o |U_o}{8}, \tag{A.3}$$

where f_o is the oil friction factor and U_o is the local water velocity, and

$$f_o = \begin{cases} 64/Re_o = 64/(\rho_o D_{ho} U_o/\mu_o) & \text{for } Re_o \leqslant 1500 \\ \left\{-1.8\mathrm{Log}_{10}\left[\frac{6.9}{Re_o} + \left(\frac{e}{3.7D_{ho}}\right)^{1.1}\right]\right\}^{-2} & \text{for } Re_o > 1500, \end{cases} \tag{A.4}$$

where Re_o is the oil Reynolds number, D_{ho} is the oil hydraulic diameter, μ_o is the oil viscosity. The friction factor f_w in Eq. (A.2) and f_o in Eq. (A.4) are evaluated using adjustable definitions of the equivalent hydraulic diameters (Brauner and Maron, 1992a,b),

for $U_w > U_o$,

$$D_{hw} = \frac{4A_w}{(S_w + S_i)} \quad \text{and} \quad D_{ho} = \frac{4A_o}{S_o} \tag{A.5)and(A.6}$$

for $U_w < U_o$

$$D_{hw} = \frac{4A_w}{S_w} \quad \text{and} \quad D_{ho} = \frac{4A_o}{(S_o + S_i)}. \tag{A.7)and(A.8}$$

According to Trallero (1995), the interfacial shear stress can expressed as

$$\tau_i = \tau_{i,smooth} + \tau_{i,wavy}, \tag{A.9}$$

where

$$\tau_{i,smooth} = f_i \rho_f \frac{(U_w - U_o)^2}{8} \tag{A.10}$$

and considering the sheltering hypothesis,

$$\tau_{i,wavy} = \rho_f (U_w - U_o)^2 C_s = f(h_w, x) \quad \text{and} \tag{A.11}$$

for $U_w > U_o$

$$f_i = f_w \quad \text{and} \quad \rho_f = \rho_w, \quad \text{and} \tag{A.12)and(A.13}$$

for $U_w < U_o$

$$f_i = f_o \quad \text{and} \quad \rho_f = \rho_o. \tag{A.14)and(A.15}$$

Note that $\tau_{i,smooth}$ considers only the interfacial friction when the interface is smooth. The wave effects are incorporated into the model via $\tau_{i,wavy}$ and the parameter C_s must be evaluated empirically. It was used the parameter $C_s = 0.073$, which was adjusted by Trallero (1995).

References

Alkaya, B., Jayawardena, S.S., Brill, J.P., 2000. Oil water flow patterns in slightly inclined pipes. In: Proceedings of ETCE/OMAE2000 Joint Conference, New Orleans, 14–17 February.

Angeli, P., Hewitt, G.F., 1998. Pressure gradient in horizontal liquid–liquid flows. Int. J. Multiphase Flow 24, 1183–1203.

Bannwart, A.C., Rodriguez, O.M.H., de Carvalho, C.H.M., Wang, I.S., Obregon Vara, R.M., 2004. Flow patterns in heavy crude oil–water flow. J. Energy Resour. Technol.-Trans. ASME 126, 184–189.

Brauner, N., 2001. The prediction of dispersed flows boundaries in liquid/liquid and gas/liquid systems. Int. J. Multiphase Flow 27, 885–910.

Brauner, N., Maron, D.M., 1992a. Flow pattern transitions in two-phase liquid–liquid flow in horizontal tubes. Int. J. Multiphase Flow 18, 123–140.

Brauner, N., Maron, D.M., 1992b. Stability analysis of stratified liquid–liquid flow. Int. J. Multiphase Flow 18, 103–121.

Brauner, N., Maron, D.M., 1999. Classification of liquid–liquid two-phase flow systems and the prediction of flow pattern maps. In: Proceedings of 2nd International Symposium on Two-Phase Flow Modeling and Experimentation—ISTP'99 2, Pisa, Italy, pp. 747–754.

Elseth, G., 2001. An experimental study of oil–water flow in horizontal pipes. Ph.D. thesis. The Norwegian University of Science and Technology, Porsgrunn.

Fairuzov, Y.V., 2001. Stability analysis of stratified oil/water flow in inclined pipelines. SPE Production and Facilities, 14–21 February.

Fairuzov, Y.V., Arenas-Medina, P., Verdejo-Fierro, J., Gonzales-Islas, R., 2000. Flow pattern transitions in horizontal pipelines carrying oil–water mixtures: full-scale experiments. J. Energy Resour. Technol.-Trans. ASME 122, 169–175.

Haaland, S.E., 1983. Simple and explicit formulas for the friction factor in turbulent pipe flows. Fluids Eng., 89–90.

Lovick, J., Angeli, P., 2001. Two-phase liquid flows at the partially dispersed flow regime. In: Proceedings of 4th International Conference of Multiphase Flow—ICMF'01, New Orleans, 27 May–1 June.

Lovick, J., Angeli, P., 2004. Experimental studies on the dual continuous flow pattern in oil–water flows. Int. J. Multiphase Flow 30, 139–157.

Nädler, M., Mewes, D., 1997. Flow induced emulsification in the flow of two immiscible liquids in horizontal pipes. Int. J. Multiphase Flow 23, 55–68.

Oddie, G., Shi, H., Durlofsky, L.J., Aziz, K., Pfeffer, B., Holmes, J.A., 2003. Experimental study of two and three phase flows in large diameter inclined pipes. Int. J. Multiphase Flow 29, 527–558.

Petalas, N., Aziz, K., 2000. A mechanistic model for multiphase flow in pipes. J. Can. Pet. Technol. 39, 43–55.

Rodriguez, O.M.H., Bannwart, A.C., 2004. Flow patterns in vertical and horizontal heavy crude oil–water two-phase flow and stability analysis of core-annular flow. In: Proceedings of 5th International Conference on Multiphase Flow—ICMF'04, Yokohama, Japan, 30 May–4 June.

Rodriguez, O.M.H., Mudde, R.F., Oliemans, R.V.A., 2004. Inversion of multiphase flow models for multiphase well logging: larger diameters and lightly inclined pipes. In: Proceedings of 4th North American Conference on Multiphase Technology, Banff, Canada, 3–4 June.

Sotgia, G., Tartarini, P., 2001. Experimental and theoretical investigation on pressure drop reductions in oil water flows. In: Proceedings of 4th International Conference of Multiphase Flow—ICMF'01, New Orleans, 27 May–1 June.

Trallero, J.L., 1995. Oil–water flow patterns in horizontal pipes. Ph.D. thesis, The University of Tulsa, Tulsa, Oklahoma.

Trallero, J.L., Sarica C., Brill, J.P., 1997. A study of oil/water flow patterns in horizontal pipes. SPE Production and Facilities (SPE 36609), August.

Valle, A., Utvik, O.H., 1997. Pressure drop, flow pattern and slip for two-phase crude oil/water flow: experiments and model predictions. In: Proceedings of International Symposium on Liquid–Liquid Two Phase Flow and Transport Phenomena, Antalya, Turkey.

Wallis, G.B., 1969. One-Dimensional Two-Phase Flow. MacGraw-Hill, New York.